



AIAA 2005-4353

Unsteady Navier-Stokes Rocket Nozzle Flows

I-Shih Chang
The Aerospace Corporation
El Segundo, California

Chau-Lyan Chang
NASA Langley Research Center
Hampton, Virginia

Sin-Chung Chang
NASA Glenn Research Center
Cleveland, Ohio

**41st AIAA/ASME/SAE/ASEE
Joint Propulsion Conference and Exhibit
11-13 July 2005
Tucson, Arizona**

Unsteady Navier-Stokes Rocket Nozzle Flows

I-Shih Chang*

The Aerospace Corporation, El Segundo, California 90245

Chau-Lyan Chang**

NASA Langley Research Center, Hampton, Virginia 23681

Sin-Chung Chang***

NASA Glenn Research Center, Cleveland, Ohio 44135

The space-time conservation element/solution element (CE/SE) method in conjunction with an unstructured mesh generator is applied to solve unsteady Navier-Stokes (N-S) rocket nozzle flows. The space-time CE/SE method considers space and time as a single entity, preserves both local and global flux conservation in the solution procedure, and provides accurate, unsteady analysis results for both the N-S (viscous) and the Euler (inviscid) nozzle flows. No computational difficulty is encountered with the unstructured mesh using high-aspect-ratio triangular elements in the viscous boundary layer. The method automatically captures distinctive features of flow separations and complicated wave interaction patterns of shear layers, incident shocks, reflected shocks, slipstreams, Mach disks, and traveling vortex rings during unsteady flow development in the nozzle and in the near field of its exhaust jet without using any turbulence model or flow separation model. Detailed calculations are carried out for overexpanded flows inside the JPL axisymmetric, convergent-divergent nozzle. Salient characteristics of the unsteady N-S flows compared with those of the steady-state flows are revealed. Excellent agreement is obtained between analysis results and experimental test data at various ambient pressure conditions.

1. Introduction

Nozzle design constitutes an important phase of rocket development. The performance of a rocket depends heavily on rocket nozzle's effectiveness in converting thermal energy to kinetic energy. For many years, traditional methods, namely the method of characteristics, finite-difference, finite-volume, and finite-element methods, have been used successfully to analyze steady-state flow-fields inside rocket nozzles and their associated jets. However, these methods cannot solve unsteady flow-fields adequately, because the algorithms of the traditional methods consider the flux conservations in the spatial domain and do not have provisions for flux conservations in the time domain. Numerical results obtained from the application of these traditional methods for solutions of unsteady rocket nozzle and jet flows can be of questionable value.

Nozzle design including operational capability and integrity of thrust vector control (TVC) components has been mainly based on the results from a steady-state flow analysis. Empirical relations for approximate treatment of the unsteady effect are then used to supplement the results obtained from

the steady-state flow analysis. But the outcome of this design approach is often unsatisfactory. In-flight anomalous events associated with a higher than expected maximum load on TVC actuator during ignition transient have been observed for solid rocket motors developed and qualified under this design approach (Ref. 1). The ultra-short dynamic events associated with flows that follow opening of the propellant injection valve and initiation of ignition inside a liquid rocket engine have caused severe pressure wave oscillation, erroneous ignition sequencing, combustion instability, and ensuing launch failures (Ref. 2). Severe unsteady pressure loading on nozzle components during the ignition transient have also caused in-flight rocket nozzle component damage and possible launch failures (Refs. 3-4). Lateral ignition impulse in solid rocket motors has been observed to cause a pointing error in spin stabilized upper-stage vehicle (Ref. 5) and overload of the design capability of the attaching brackets associated with the nozzle actuating struts (Ref. 6). Understanding and accurately analyzing unsteady flow development inside the nozzle are important to rocket nozzle design improvement.

This study is the extension of the previous works on the solution of unsteady Euler inviscid nozzle and jet flows (Refs. 7-8) to unsteady Navier-Stokes (N-S) viscous flows. The study applies a new paradigm, the space-time conservation element/solution element (CE/SE) method (Refs. 9-11), in conjunction with an unstructured mesh generator (Refs. 12-14), to solve unsteady N-S rocket nozzle and its near-field exhaust jet flows. Since modern rocket nozzles usually have high area ratios for enhanced rocket performance, these nozzles will unavoidably operate in an overexpanded environment during

* Distinguished Engineer, Vehicle Systems Division

** Research Scientist, Research and Technology Directorate

***Senior Research Scientist, Propulsion Systems Division

lift-off. In an overexpanded environment the flow pressure at the exit plane of the nozzle is lower than the ambient pressure, and the flow will separate from the nozzle wall as a result of viscous boundary-layer, ambient pressure field, and nozzle core flow interactions. Therefore, emphasis of the present study will be on flow separation phenomena observed inside the divergent section of the nozzle in an overexpanded environment. Detailed calculations are carried out for the unsteady N-S flows inside the classic Jet Propulsion Laboratory (JPL) nozzle (Refs. 15-16). Salient characteristics of the unsteady N-S flows in the nozzle and its near-field exhaust jet are revealed. The results of the N-S flow analysis are compared with those of the Euler flow analysis. Flow separation phenomena and complicated wave interaction patterns in the nozzle at various ambient pressure conditions are presented.

2. The Space-Time CE/SE Method

The space-time CE/SE method, introduced by S.-C. Chang (Refs. 9-11) for solving the physical conservation laws, represents a new approach for accurately computing inviscid and viscous unsteady flows. Unlike traditional approaches, this new explicit numerical method offers discretized solutions for physical conservation laws without resorting to artificial splitting and reconstruction of the flux vectors at the element interface. The method has been shown (Refs. 17-19) to produce accurate results for a broad spectrum of flows in computational aero-acoustics (CAA) and in computational fluid dynamics (CFD) from very low to hypersonic speeds. In contrast to traditional CFD methods, the space-time CE/SE method has the following salient features:

- It treats space and time synergistically by constructing the discretized mesh in a domain defined by both temporal and spatial coordinates. Unbiased time treatment ensures consistent temporal numerical accuracies.
- It preserves both local and global flux conservation in space and time. Staggered solution elements and conservation elements allow the flux integration to be performed without ad-hoc reconstructions (usually through interpolation or extrapolation of dependent variables or fluxes) at the element interface. In the presence of discontinuities, no Riemann solver is required at the interface. This implies that no dimensional splitting or multi-dimensional upwind formulation for the flux vector is necessary. It can be proven mathematically that flux conservation is perfectly preserved in the discretized space for each conservation element as well as the entire domain for the CE/SE method. Moreover, flux conservation in time as a result of synergistic temporal and spatial treatments offers many attractive features such as higher temporal accuracy, easier boundary condition treatment, and better approximation for numerical models that require a high degree of conservation (i.e., large-eddy simulations). The method uses 2-D triangles and 3-D tetrahedrons as the simplest building blocks for unstructured spatial meshes. Extensions to quadrilateral or

hexahedral elements can be formulated as a special case.

- It uses simple flux balance for boundary condition implementation. In conventional CFD methods, characteristic variables (Riemann invariants) in the direction normal to the boundary are used to manually limit the traveling directions of characteristic information. For multi-dimensional problems, this one-dimensional characteristic splitting is not exact and introduces additional errors that cause boundary reflections. A buffered domain or sponge layer near the boundary is usually introduced to alleviate boundary reflections. In contrast, in the CE/SE method a simple extrapolation boundary condition without a buffered domain works well for non-reflective boundary conditions. This nice property is associated with the conservation of flux along the temporal direction. Global flux formulation along all directions allows information to propagate in time and exit the domain without incurring significant boundary reflections even with a simple extrapolation boundary condition. In fact, it can be shown that propagation of erroneous information associated with inappropriate boundary conditions is only confined to the close vicinity of the source. For very small-amplitude perturbations, noticeable reflection at the boundary may still be observed. However, it can be eliminated by a relatively small buffered domain because of "local" nature of boundary reflections in the space-time CE/SE method.
- It is constructed based on a zero-dissipation "a-scheme" (Ref. 9). Numerical dissipation is added to provide numerical stability of the Euler or N-S equations. The existence of a zero-dissipation "a-scheme" offers a reference point to control the amount of numerical dissipation being added. For high-fidelity computations such as those in CAA or direct numerical simulations, better control of numerical dissipation can significantly increase the solution accuracy. Combining with the ability to handle flow discontinuities without using the ad-hoc multi-dimensional Riemann solvers, the CE/SE method offers an accurate scheme to compute complex wave phenomena in the presence of shocks.
- It does not require any preconditioning of the governing equations to preserve the solution accuracy when applied to low Mach number flows. Solving low speed flows using the compressible governing equations suffers from error accumulation associated with the disparity in the eigenvalues of the system. Modification of the equations to alter the eigenvalues is often required to improve convergence rate and solution accuracy. It has been shown that the CE/SE method can provide highly accurate solutions after long time integration without any preconditioning techniques. The convergence rate remains slow because of the presence of the low eigenvalues, but the error accumulation problem does not exist in the CE/SE method.

The space-time CE/SE method has also been applied successfully to solve problems in electromagnetic wave scatter-

ing and antenna radiation, magnetic induction field and MHD vortex, crystallization process, chromatographic adsorption, thin-fluid-film tribology, and the Saint Venant equations in hydraulic engineering (Refs. 20-25). The theoretical basis of the space-time CE/SE method is given in Refs. 9-11 and will not be repeated here. The following section briefly describes the issues associated with the N-S flow computations.

3. Navier-Stokes Flow Computations

Numerical formulations of the CE/SE method for the Euler equations are directly applicable to the Navier-Stokes equations provided that several important issues are properly addressed. Firstly, viscous terms must be added to the flux vectors. These terms involve derivatives of dependent variables. Within the framework of the CE/SE method, these derivatives are assumed to be constant over the solution element. To account for variations of derivatives within each solution element, higher derivatives must be introduced and evaluated. As a first approximation and to avoid complex numerical treatments, the constant derivatives at the conservation element interface for the evaluation of viscous terms are used. In the N-S calculations, the discretized equations from the Euler formulation are used with flux vectors evaluated by summing the inviscid and viscous terms simultaneously.

The second issue related to viscous calculations is the near wall mesh stretching. Without proper mesh clustering near the solid wall boundary, effects of viscosity cannot be properly accommodated. High-aspect-ratio mesh near the solid wall may slow down convergence and significantly affect the robustness of the N-S solver. For steady-state problems, a constant CFL number (local time-stepping) can be specified to accelerate convergence. For unsteady calculations with a constant time step for all elements, the local CFL (Courant-Friedrichs-Lewy) number varies from 1 (to maintain numerical stability) near the wall to a very small value in the coarse mesh region. A small CFL number implies a large numerical dissipation for the original CE/SE method (Ref. 9). The disparity in CFL number thus may result in adverse effects on the solution accuracy. The newly devised Courant number insensitive CE/SE scheme by S.-C. Chang (Refs. 10-11) is aimed at controlling numerical dissipation for small CFL numbers and through which a uniform numerical dissipation may be achieved for a highly nonuniform mesh. Alternatively, a local time-stepping procedure that preserves the time accuracy (Ref. 18) may also be used. In this paper, the Courant number insensitive scheme and local time-stepping are used to ensure solution accuracy. The third issue is related to the viscous wall boundary conditions. No-slip boundary condition and thermal boundary conditions are enforced in a ghost cell adjacent to the solid wall. Reynolds number dependent viscous flux formulation (Ref. 26) was not used, because it does not guarantee correct velocity derivatives near the wall. For high-aspect-ratio mesh adjacent to the solid wall, the Courant number insensitive scheme and very small mesh spacing are used to control numerical dissipations and thus alleviate

numerical instability caused by large gradient.

To facilitate high-fidelity unsteady computations with an unstructured mesh, a 2-D/3-D Navier-Stokes code (named *ez4d*) based on the space-time CE/SE method was developed by C.-L. Chang (Ref. 27). The *ez4d* code is written in the C++ programming language with state-of-the-art object oriented and generic programming techniques using the Standard Template Library (STL). The core solver is based on an unstructured topology using triangular or quadrilateral mesh for 2D flows and tetrahedral or hexahedral mesh for 3D flows. Input interfaces to process a 2D or 3D structured mesh are also included in *ez4d*. A 2D/3D multi-block structured mesh can thus be handled by the code. Domain decomposition based on the popular Metis library is used to partition an unstructured mesh for parallel processing. Both multi-thread and Messaging Passing Interface (MPI) are implemented in *ez4d* to facilitate parallel processing of very large meshes. The code has been validated against other existing structured and unstructured CFD codes. The solution accuracy for viscous calculations has been verified by comparing the results from *ez4d* code with exact solutions of Blasius boundary layer flows and Stokes's first and second problems (Ref. 28) and with test data for subsonic/supersonic blunt body flows and acoustic wave simulations. All the results presented in this paper have been generated by using the *ez4d* code.

4. Computational Mesh for JPL Nozzle

The compressible flow inside the JPL axisymmetric convergent-divergent nozzle with a 45° entrance and a 15° exit straight wall tangent to a circular throat (with ratio of throat radius of curvature to throat height = 0.625) is a classic nozzle flow problem, which has been analyzed by many researchers using various traditional CFD methods for steady-state flows. The unsteady behavior of the flow inside the JPL nozzle and inside other rocket nozzles of practical importance is largely unknown, mainly because of the difficulty in obtaining accurate unsteady flow solutions. Reference 7 successfully applied the space-time CE/SE method to solve unsteady Euler flows inside the JPL and the Titan IVB SRMU nozzle and investigate the effect of different time-dependent, inlet flow conditions on the transient flow behavior and its dynamic loading on the nozzle wall. The present study applied the space-time CE/SE method to solve the full unsteady N-S equations for overexpanded flows inside the JPL nozzle.

The 2D unstructured mesh generation methodology for Euler flows was extended to N-S flows utilizing the method shown in Refs. 12-14. Very fine mesh sizes are required to resolve the viscous layers near the nozzle walls in the N-S calculations. An automated procedure was then developed for generating unstructured meshes efficiently, incorporating boundary conditions correctly, and ensuring transmission of mesh files to the N-S solver seamlessly. For overexpanded nozzle flow calculations, it is necessary that a portion of exhaust jet from the nozzle be included in the computational

domain. The exhaust jet must be included because the flow separation inside the nozzle depends strongly on the ambient pressure condition. The flow is highly nonuniform at the nozzle exit plane and cannot be specified a priori, especially during unsteady flow development. Solving the exhaust jet along with the nozzle flow would allow ambient pressure conditions to be specified further downstream to mimic a more realistic environment. Figure 1 shows that the unstructured mesh covers a portion of the exhaust jet flow field up to 9 times the nozzle exit diameter in the axial and 10 times in the radial directions. The unstructured mesh for one-half of the physical region consists of 208,027 elements and 108,082 nodes and is obtained from the automated, unstructured mesh generation procedure for N-S flows. Shown in the same figure is an enlarged view of clustered meshes near the nozzle wall for the N-S flow computations.

Initially, the physical region contains an ideal gas ($\gamma = 1.4$) at a quiescent ambient condition. Time marching starts when the one-D flow (with density ρ_1 , speed u_1 , and pressure P_1) enters the nozzle inlet plane on the left side boundary of the physical region. A reflective boundary condition is imposed on the centerline of symmetry. On the solid wall, a no-slip or reflective boundary condition is specified for the N-S or the Euler calculations, respectively. A non-reflective boundary condition is imposed on the exit plane of the exhaust jet flow located on the right (exit) boundary of the physical region. The ambient condition is applied on the outer radial boundary of the exhaust jet. The Prandtl number is 0.72, and the Reynolds number per unit length is 10,000 for the N-S flows.

5. Results and Discussions

The computed unsteady N-S flow fields for the JPL nozzle and its exhaust jet at 1,000th, 2,000th, and 10,000th marching steps at an ambient condition $P_a/P_t = 0.20$ are given in the gas density, Mach number, and pressure contour plots of Fig. 2, 3, and 4, respectively. Here P_a/P_t is the ratio of the ambient pressure on the outer radial boundary of the exhaust jet to the total pressure at the nozzle inlet plane. In the contour plots, the density is normalized by ρ_1 , and the pressure is normalized by $\rho_1 u_1^2$, where ρ_1 is the reference gas density and u_1 is the reference flow speed evaluated from the one-dimensional isentropic state at the nozzle inlet plane. At $P_a/P_t = 0.20$ the nozzle flow field is essentially established after 10,000 marching steps, although the exhaust jet flow field is still undergoing changes. Many more marching steps are needed to reach established jet flow field as shown in Ref. 8.

The contour plots reveal vortex rings and complicated wave interaction patterns appearing inside the nozzle and traveling down the exhaust jet during unsteady flow development. These flow features are captured automatically from the unsteady N-S flow solutions using the space-time CE/SE method. A steady-state analysis would not be able to unveil such important features of the transient flow. The traveling vortex rings and wave interaction patterns produce nonuni-

form, transient dynamic pressure loading on the nozzle and exit cone wall and on the thrust vector control components and could influence rocket nozzle structural integrity and operational safety during the ignition transient. The important corollary of this observation is that traditional methods, which provide the computed flow solutions in good agreement with steady-state test data could be erroneously considered to be applicable to the unsteady flow situation. As discussed in Ref. 7, a rocket nozzle based on the design approach with an incorrect unsteady flow-field and a grossly underestimated magnitude of transient dynamic loading on the nozzle wall would have a margin of safety significantly lower than that projected in the actual flight operation.

Figures 2, 3, and 4 also show that, without utilizing any turbulence model or flow separation model, the unsteady flow separation phenomena evolve automatically during the solution of the unsteady N-S equations. Traveling vortex rings and complicated wave interaction patterns, including shear layers, incident shocks, reflected shocks, slipstreams, and Mach disks during unsteady flow development in the divergent section of the nozzle and in the near field of the exhaust jet appear naturally in the solution using the space-time CE/SE method.

It is well known that the Euler flow calculations provide adequate solutions for under-expanded nozzle flows, as far as the pressure loading on the wall is concerned. For overexpanded nozzle flows, however, high ambient pressure induces an adverse pressure gradient, which prevents further flow expansion in the nozzle, and flow separation occurs near the nozzle wall. The flow separation is mainly the result of viscous boundary-layer, ambient pressure field, and nozzle core flow interactions and cannot be solved by the Euler flow analysis, even though flow models (e.g. Refs. 29-31) have been devised in the past in an attempt to predict flow separation from an analysis without solving the viscous boundary layer near the nozzle wall. The flow separation models may work locally for some particular nozzle configurations under some specified circumstances and should not be extrapolated to other uncharted flow situations. To illustrate this point, Fig. 5 compares the density, Mach No., and pressure contours from the N-S flow analysis with those from the Euler flow analysis using the same computational mesh given in Fig. 1. The comparison clearly reveals striking differences in the wave interaction patterns of the N-S flow from those of the Euler flow. The results obtained from an inviscid flow model for predicting flow separation in an overexpanded nozzle should be treated with caution, especially, when they are applied to unsteady flow situations. Accurate evaluation of transient rocket nozzle thrust degradation caused by flow separation warrants the solution of the full, unsteady N-S flow equations such as the one carried out in this study.

Figure 6 shows the mesh detail and N-S flow-field near flow separation point at $P_a/P_t = 0.20$. The gas density, Mach No., and pressure contours contain a complicated wave inter-

action pattern, including the shear layer, the incident shock, the reflected shock, the slipstream, and the Mach disk, downstream of the flow separation point. The velocity vector plot reveals that there is clearly a recirculation region near the nozzle wall downstream of the flow separation point, and the flow in front of the incident shock and the Mach disk is highly nonuniform. Significant differences in magnitude and direction of velocity vectors upstream and downstream of the incident shock and the Mach disk can be easily discerned in the velocity vector and in the contour plots. The contour plots illustrate distinctly the appearance of shear layers, which include the viscous boundary layer and flow separation boundary near the wall, and the slipstream, which emanates from the triple point of the Mach configuration. Across the shear layers and slipstream, gas pressure is constant, but density and velocity are different. The computed results also show that the pressure on the wall stays fairly constant at the ambient condition downstream of the flow separation point.

Figure 7 shows the computed gas density and Mach number contours for established N-S flows in the JPL nozzle at three ambient-to-nozzle chamber pressure ratios, namely, $P_a/P_t = 0.33, 0.20,$ and 0.10 . Figure 8 gives the computed pressure contours in the nozzle and pressure distributions at the nozzle wall and at the centerline at the same ambient-to-nozzle chamber pressure ratios. It is obvious that, for a fixed nozzle chamber pressure, the flow separation point moves downstream toward the nozzle exit plane as the ambient pressure is decreased. Not so obvious is the fact that the CFL number needs to be reduced accordingly as well, in order to obtain stable solutions. For the present calculations the CFL numbers are 0.5 for $P_a/P_t = 0.33$, 0.4 for $P_a/P_t = 0.20$, and 0.3 for $P_a/P_t = 0.10$. Remarkable differences in the wave interaction patterns downstream of the Mach Disk are observed at different ambient pressure conditions. At $P_a/P_t = 0.33$ the subsonic core flow downstream of the Mach disk extends well into the nozzle exit plane, and the constant pressure boundary near the nozzle wall remains rather straight and is not altered by the interacting weak reflected shock. At $P_a/P_t = 0.20$ the core flow downstream of the Mach disk undergoes a clear subsonic-to-supersonic flow expansion, and the constant pressure boundary near the nozzle wall is deflected and curved by a stronger intersecting reflected shock. Inside the nozzle the flow is highly nonuniform, and the complicated wave interaction pattern including the incident shock, the reflected shock, the slipstream, and the Mach disk appear automatically in all the results of computation for different ambient-to-nozzle chamber pressure ratios.

Figure 9 shows the comparison of results from the N-S and the Euler flow analyses with the test data (Refs. 15-16) at $P_a/P_t = 0.20$. The pressure distributions (normalized by the total pressure at the nozzle inlet plane in this and next figures) at the nozzle wall and at the centerline of symmetry from the N-S flow analyses agree well with those from the test data. The computed location of flow separation on the nozzle wall also agrees well with the test data. The results from the Euler flow

analysis are plotted in the same figure for easy comparison. The Euler flow analysis provides adequate pressure distribution at the nozzle wall and at the centerline of symmetry upstream of the flow separation point, but is not appropriate for solving the flow in the divergent section of high area ratio where flow separation occurs in overexpanded flow situations. This is the reason that the previous Euler flow analysis (Ref. 7) was performed only for the JPL nozzle with a truncated exit cone.

Figure 10 shows the comparison of results from the N-S flow analysis with test data (Refs. 15-16) at several different ratios of ambient pressure to nozzle chamber pressure. The computed pressure distributions and locations of flow separation at the nozzle wall from the N-S flow analyses agree well with those from the test data at various ambient-to-chamber pressure ratios. There are no pressure measurements at the centerline of symmetry in the divergent section of the nozzle except those near the nozzle throat (Ref. 16) given in Fig. 9. For most ambient-to-chamber pressure ratios the established flow condition is reached after 10,000 marching steps. At high pressure-ratio ($P_a/P_t = 0.33$), however, deeper penetration and upstream movement of a subsonic pocket associated with the flow separation require that 20,000 marching steps be carried out to reach established flow conditions. Upstream of the flow separation point the established flow can be considered to be at the steady-state condition. But downstream of the flow separation point the computed pressure at the nozzle wall continues to fluctuate slightly as a result of interactions between the subsonic viscous layer and ambient pressure field. It needs to be emphasized that no turbulence model or flow separation model, as that proposed by various researchers in Refs. 29-31, is used in the present analysis. The unsteady flow separation phenomena appear automatically from the computed results.

The mesh generation and flow-field computation procedure for the unsteady N-S flow analysis have been streamlined and automated. The flow-field results are plotted directly at specified intervals during the course of the run, without the need to store massive computational results from unsteady N-S flow analysis. At the end of the run, several animation video and graphic outputs describing unsteady N-S flow-field development are obtained. To ensure that an appropriate computational mesh is used and the computed flow-field converges correctly, both the very fine mesh (208,027 elements, 108,082 nodes) and the fine mesh (124,492 elements, 65563 nodes) have been used. No significant differences in the converged nozzle flow-fields are found from using the two different meshes. The results presented in Figs. 2 through 10 are from the analysis with the very fine mesh given in Fig. 1. An unstructured mesh generation takes only a few minutes, but the unsteady N-S flow-field computation for 10,000 marching steps takes about 30 hours on a SGI Origin 3000 workstation. The generation of animation video and graphic outputs as a part of the solution from the unsteady N-S flow analysis for the JPL nozzle takes about 100 hours on the workstation.

6. Conclusions

The space-time CE/SE method, which considers space and time as a single entity and preserves both local and global flux conservation in the solution procedure, has been found in this study to provide accurate solutions to unsteady N-S rocket nozzle flows. No computational difficulty is encountered with the unstructured mesh using high-aspect-ratio triangular elements in the viscous boundary layer. Traveling vortex rings, flow separation phenomena, and complicated wave interaction patterns, including shear layers, incident shocks, reflected shocks, slipstreams, and Mach disks, in the nozzle and its exhaust jet flow-field are captured automatically during unsteady flow development, without using any turbulence model or flow separation model. The unique capability of the method to provide unsteady flow solutions cannot be overemphasized. Many unsteady rocket nozzle flow problems hitherto unsolved in space launch programs can now be analyzed with the space-time CE/SE method.

Acknowledgments

The work of the first author was supported primarily by the Aerospace IR&D under the Air Force Space and Missile Systems Center Contract No. FA8802-04-C-0001 and in part by a grant of computer time from the DoD High Performance Computing Modernization Program at NAVO and ERDC MSRCs.

References

- 1 Anon., "Titan IVB-24 Post-Flight Report - Flight Test Objectives/Performance Analysis," MCR-0012-0204, Lockheed-Martin Astronautics, April 8, 1997.
- 2 Anon., "Cause of the Failure of the 2nd Ariane Launch (L02) Found," ESA Bulletin, No. 24, Nov. 1980.
- 3 Anon., "Scout Flight Data Historical Summary," Report No. 3-34100/9R-12, LTV Aerospace, Vought Missiles and Space Division, December 1972.
- 4 Anon., "Prompt Report of M-V-4 Launch Failure," JAXA/ISAS report for cause of M-V-4 launch failure on Feb. 10, 2000 at www.isas.ac.jp/docs/sat/astro-e/prompt_report.html.
- 5 Kreiter, G. W. and C. F. Machala, "Design Considerations of Scout Upper Stages Resulting From Using Solid Rocket Motors," AIAA paper 74-1054, 10th AIAA/SAE Propulsion Conference, 21-23 October 1974.
- 6 Bowyer, J. M., Jr., G. W. Kreiter, and R. E. Petersen, "An Investigation of the Side Force that is Sometimes Observed in Rocket Motor Start-Up," AIAA paper 78-1045, 14th AIAA/SAE Propulsion Conference, 25-27 July 1978.
- 7 Chang, I-Shih, "Unsteady-State Rocket Nozzle Flows," AIAA paper 2002-3884, 38th AIAA Joint Propulsion Conf., 08-10 July 2002.
- 8 Chang, I-Shih, "Unsteady-State Underexpanded Jet Flows," AIAA paper 2002-3885, 38th AIAA Joint Propulsion Conf., 08-10 July 2002.
- 9 Chang, Sin-Chung, "The Method of Space-Time Conservation Element and Solution Element — A New Approach for Solving the Navier-Stokes and Euler Equations," *J. of Computational Physics*, 1995, pp. 295-324.
- 10 Chang, Sin-Chung, "Courant Number Insensitive CE/SE Schemes," AIAA paper 2002-3890, 38th AIAA Joint Propulsion Conf., 08-10 July 2002.
- 11 Chang, Sin-Chung, X. Y. Wang, "Multi-Dimensional Courant Number Insensitive CE/SE Euler Solvers for Applications Involving Highly Nonuniform Meshes," AIAA paper 2003-5285, 39th AIAA Joint Propulsion Conf., 20-23 July 2003.
- 12 Chang, I-Shih, "An Efficient, Intelligent Solution for Viscous Flows Inside Solid Rocket Motors," AIAA paper 91-2429, 27th AIAA Joint Propulsion Conf., Sacramento, CA, 24-26 June 1991; also 1990 JANNAF Propulsion Meeting, Anaheim, CA, *CPIA-PUB-550*, Vol. II, pp. 47-61, Oct. 1990.
- 13 Chang, I-Shih, "Adaptive, Unstructured, Finite-Element, Multimaterial, Thermal Analysis," *AIAA J. of Spacecraft and Rockets*, Vol. 30, No. 1, pp. 43-50, Jan. 1993.
- 14 Chang, I-Shih, N. R. Patel, and S. H. Yang, "Titan IV Motor Failure and Redesign Analyses," *AIAA J. of Spacecraft and Rockets*, Vol. 32, No. 4, pp. 612-618, July-Aug. 1995.
- 15 Back, L. H., P. F. Massier, and H. L. Gier, "Comparison of Measured and Predicted Flows through Conical Supersonic Nozzles, with Emphasis on the Transonic Region," *AIAA J.*, Vol. 3, No. 9, Sept. 1965, pp. 1606-1614.
- 16 Cuffel, R. F., L. H. Back, and P. F. Massier, "Transonic Flowfield in a Supersonic Nozzle with Small Throat Radius of Curvature," *AIAA J.*, Vol. 7, No. 7, July 1969, pp. 1364-1366.
- 17 Chang, Sin-Chung, X. Y. Wang, and C. Y. Chow, "The Space-Time Conservation Element and Solution Element Method—A New High-Resolution and Genuinely Multidimensional Paradigm for Solving Conservation Laws," *J. of Computational Physics* 156, 1999, pp. 89-136.
- 18 Chang, Sin-Chung, Y. Wu, V. Yang, and X. Wang, "Local Time Stepping Procedure for the Space-Time Conservation Element and Solution Element Method," accepted for publication in *Intern. J. of Computational Fluid Dynamics*.

19 Loh, C. Y., "Near Field Trailing Edge Tone Noise Computation," AIAA Paper 2003-0365, 41st AIAA Aerospace Sciences Meeting, Reno, NV, 6-9 January 2003.

20 Wang, X. Y., C. L. Chen, Y. Liu, "The Space-Time CE/SE Method for Solving Maxwell's Equations in Time-Domain," 2002 IEEE International Symposium on Antennas and Propagation and USNC/URSI National Radio Science Meeting, San Antonio, TX, 16-21 June 2002.

21 Zhang, M., S.-C. Chang, H. Lin, S. T. J. Yu, "Application of the Space-Time CE/SE Method to the Ideal Magnetohydrodynamic Equations," AIAA paper 2002-3888, 38th AIAA Joint Propulsion Conference, 9 July 2002.

22 Motz, S., A. Mitrovic, and E. D. Gilles, "Comparison of numerical methods for the simulation of dispersed phase systems," *Chemical Engineering Science*, VOL 57, Issue 20, October 2002, pp. 4329-4344.

23 Lim, Y. I., S.-C. Chang, and S. B. Jorgensen, "A novel partial differential algebraic equation (PDAE) solver: interactive space-time CE/SE method," *Computers and Chemical Engineering*, 28, 2004, pp. 1309-1324.

24 Cioc, S., F. Dimofte, T. G. Keith, D. P. Fleming, "Computation of Pressurized Gas Bearings Using the CE/SE Method," *STLE Tribology Transactions*, Vol. 46, 1, 2003, pp. 128-133.

25 Molls, T. and F. Molls, "Space-Time Conservation Method Applied to Saint Venant Equations," *J. of Hydraulic Engineering*, VOL 124, No. 5, May 1998, pp. 501-508.

26 Chang, Sin-Chung, Z. C. Zhang, S.T. John Yu, Philip C. E. Jorgenson, "A Unified Wall Boundary Treatment for Viscous and Inviscid Flows in the CESE Method," *Computational Fluid Dynamics 2000*, Edited by N. Satofuka, Springer-Verlag (2001) pp. 671-676.

27 Chang, Chau-Lyan, "Simulations of Unsteady Viscous Flows using the Space-Time CE/SE Method," AIAA Paper 2005-4358, 41st AIAA joint Propulsion Conf., 11-13 July 2005.

28 Schlichting, H., *Boundary-Layer Theory*, 6th edition, McGraw-Hill, Inc., 1968.

29 Prozan, R. J. and G. D. Luke, "CFD Prediction of Nozzle Flow Separation without Boundary Layer Resolution," AIAA paper 99-2645, 35th AIAA joint Propulsion Conf., 20-24 June 1999.

30 Summerfield, M., C. R. Foster, and W. C. Swan, "Flow Separation in Over-Expanded Supersonic Exhaust Nozzles," *Jet Propulsion*, Vol. 24, Sept.-Oct. 1954, pp. 319-321.

31 International Union of Theoretical and Applied Mechanics (IUTAM) Symposium on Unsteady Separated Flows, Toulouse, France, 8-12 April 2002.

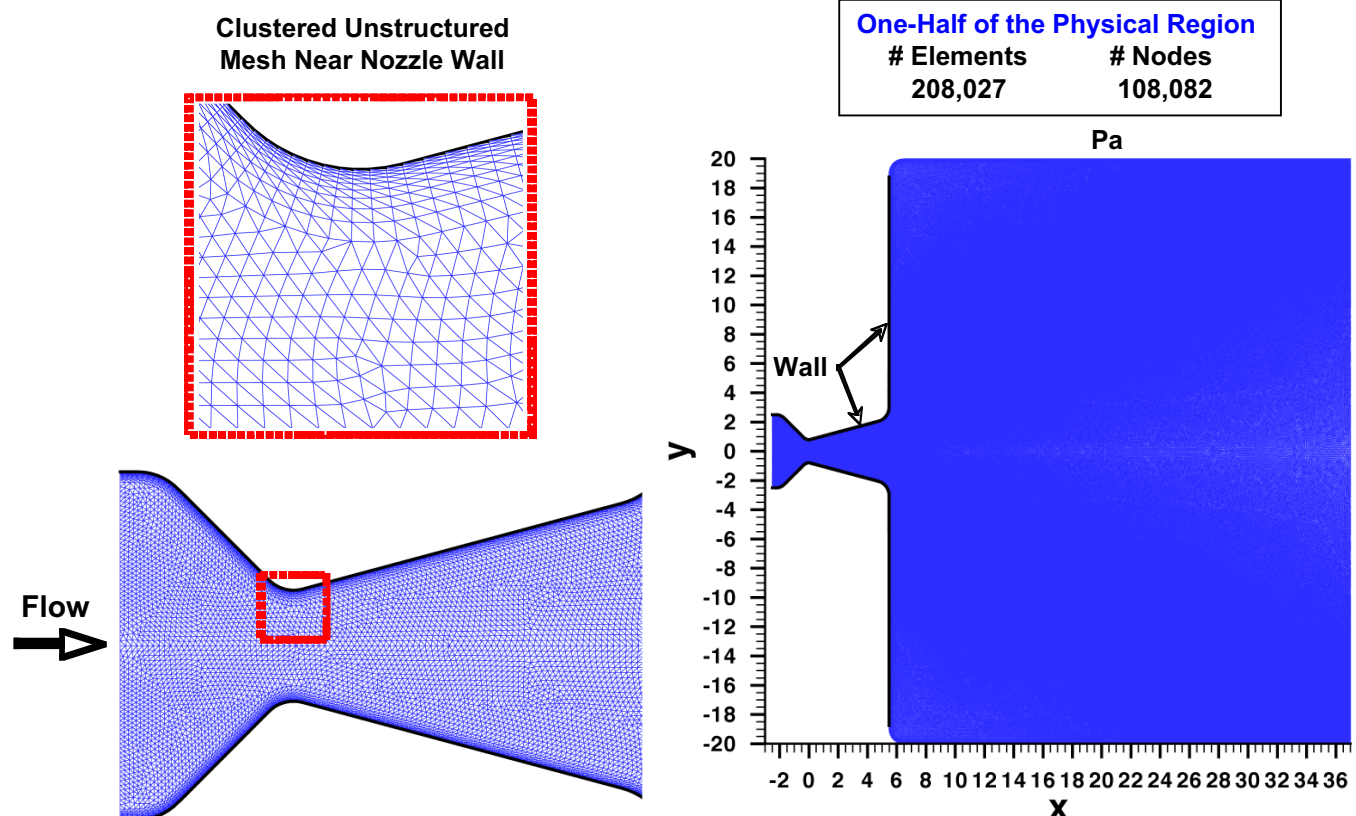


Fig. 1 Computational Mesh for the JPL Nozzle Flow

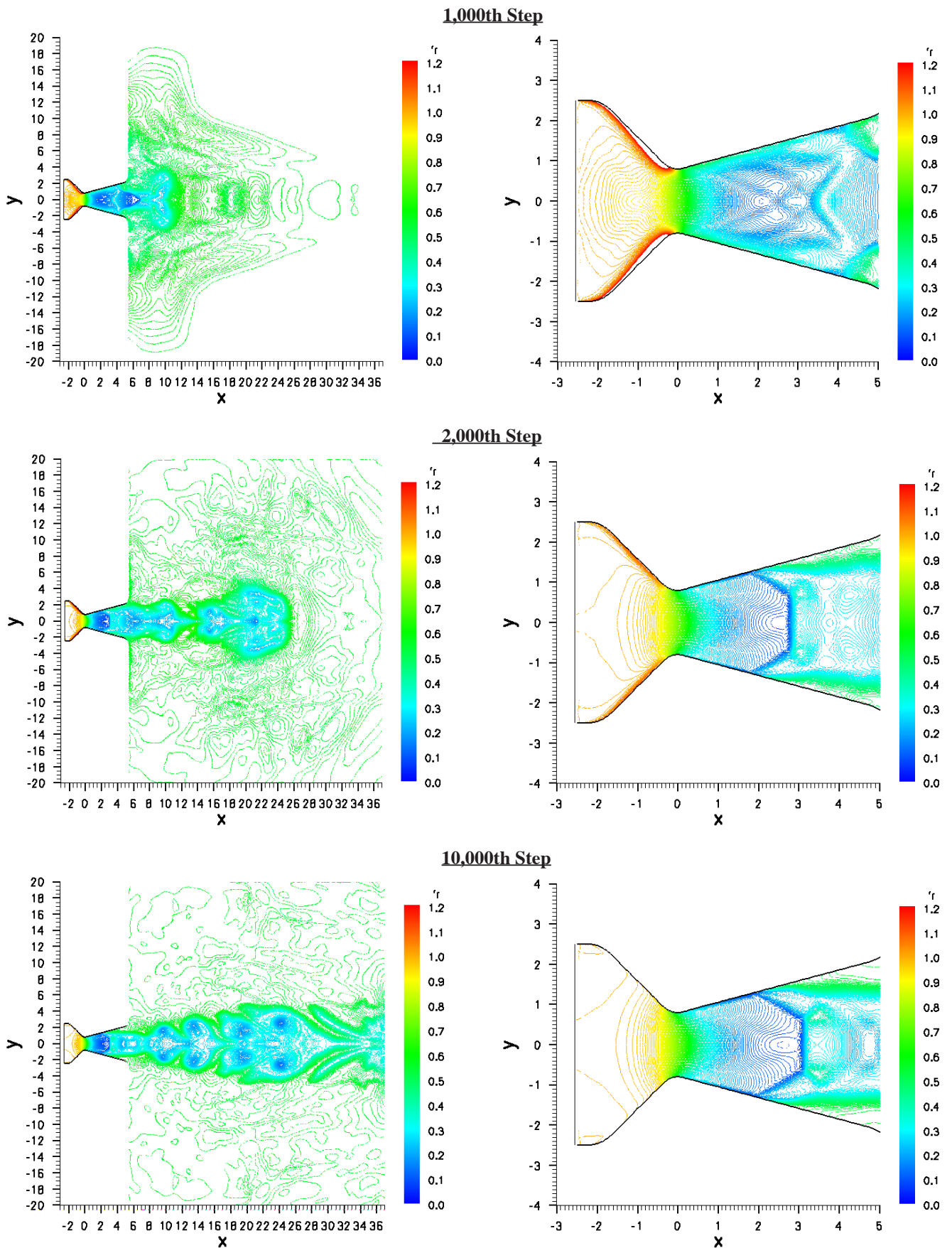


Fig. 2 Unsteady Density Contours at $Pa/Pt = 0.20$

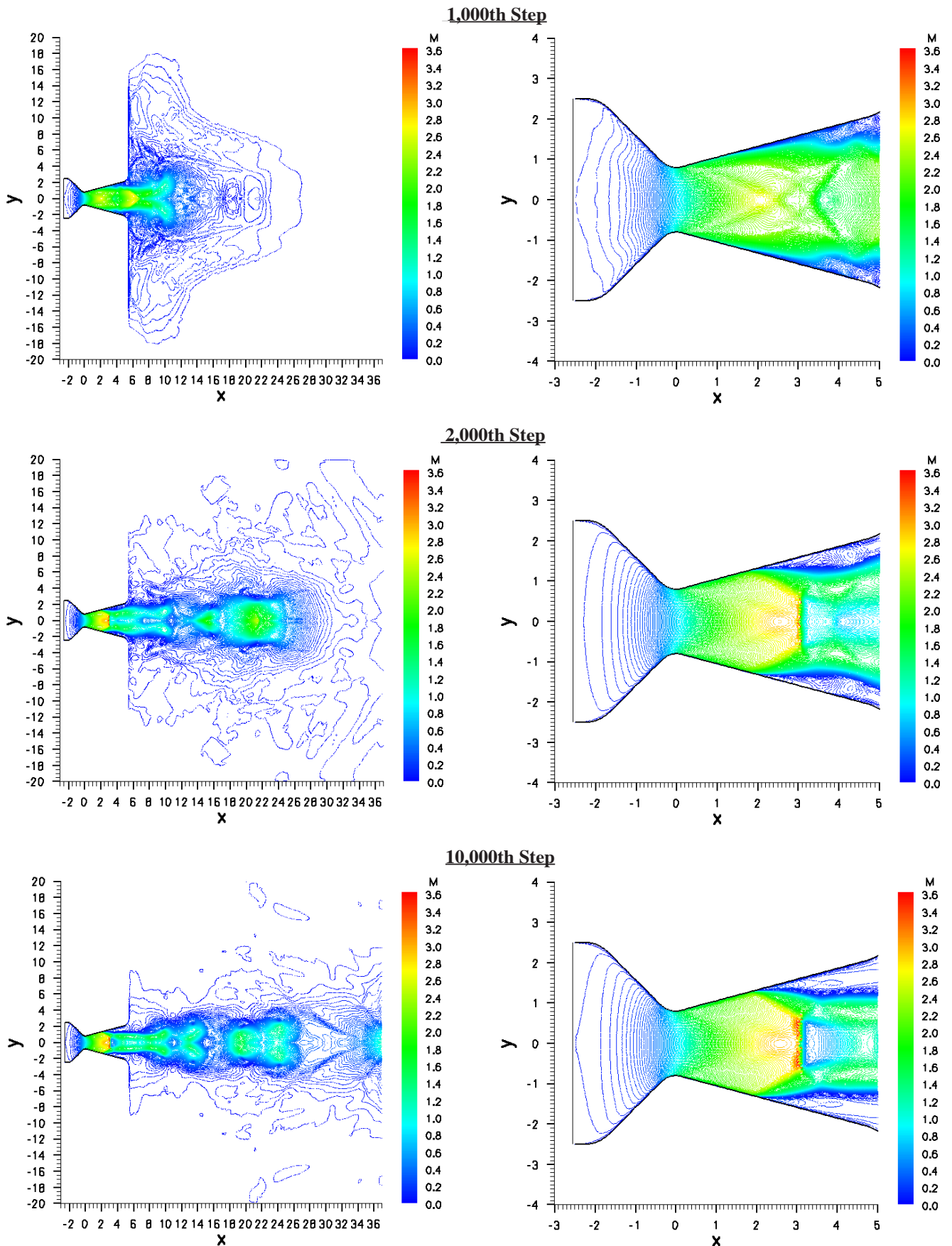


Fig. 3 Unsteady Mach No. Contours at $Pa/Pt = 0.20$

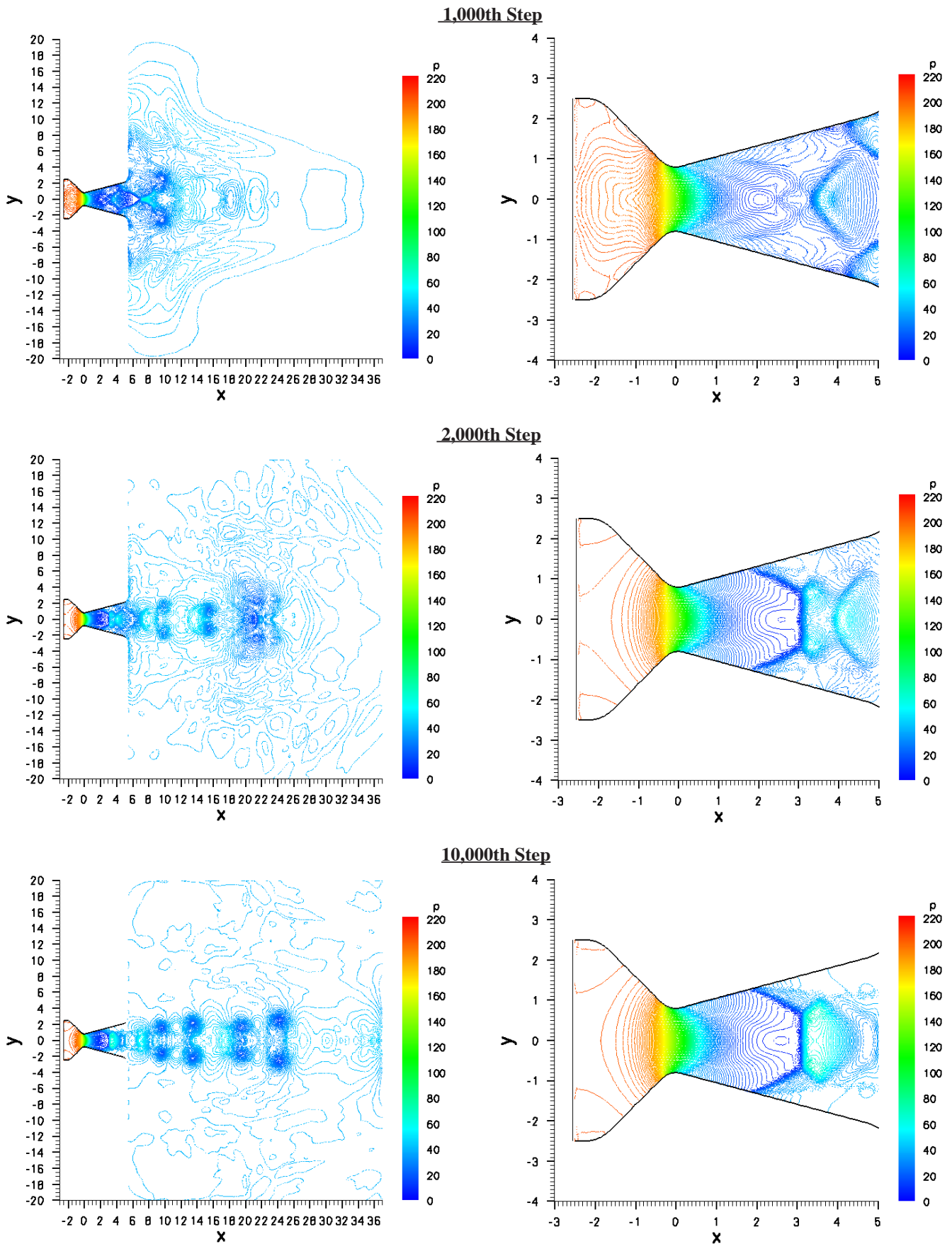


Fig. 4 Unsteady Pressure Contours at $Pa/Pt = 0.20$

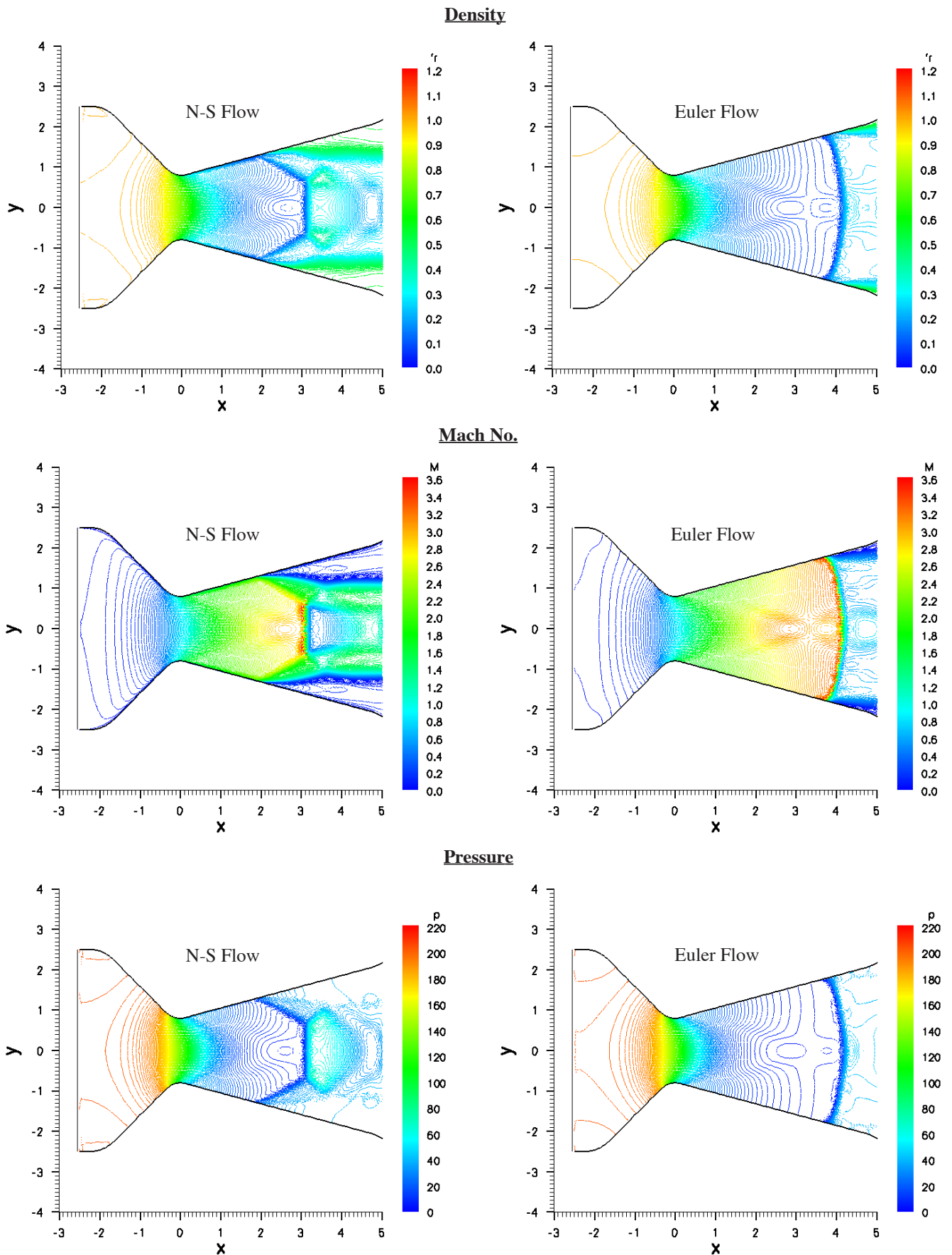


Fig. 5 Comparison of Established N-S and Euler Nozzle Flow Fields at $Pa/Pt = 0.20$

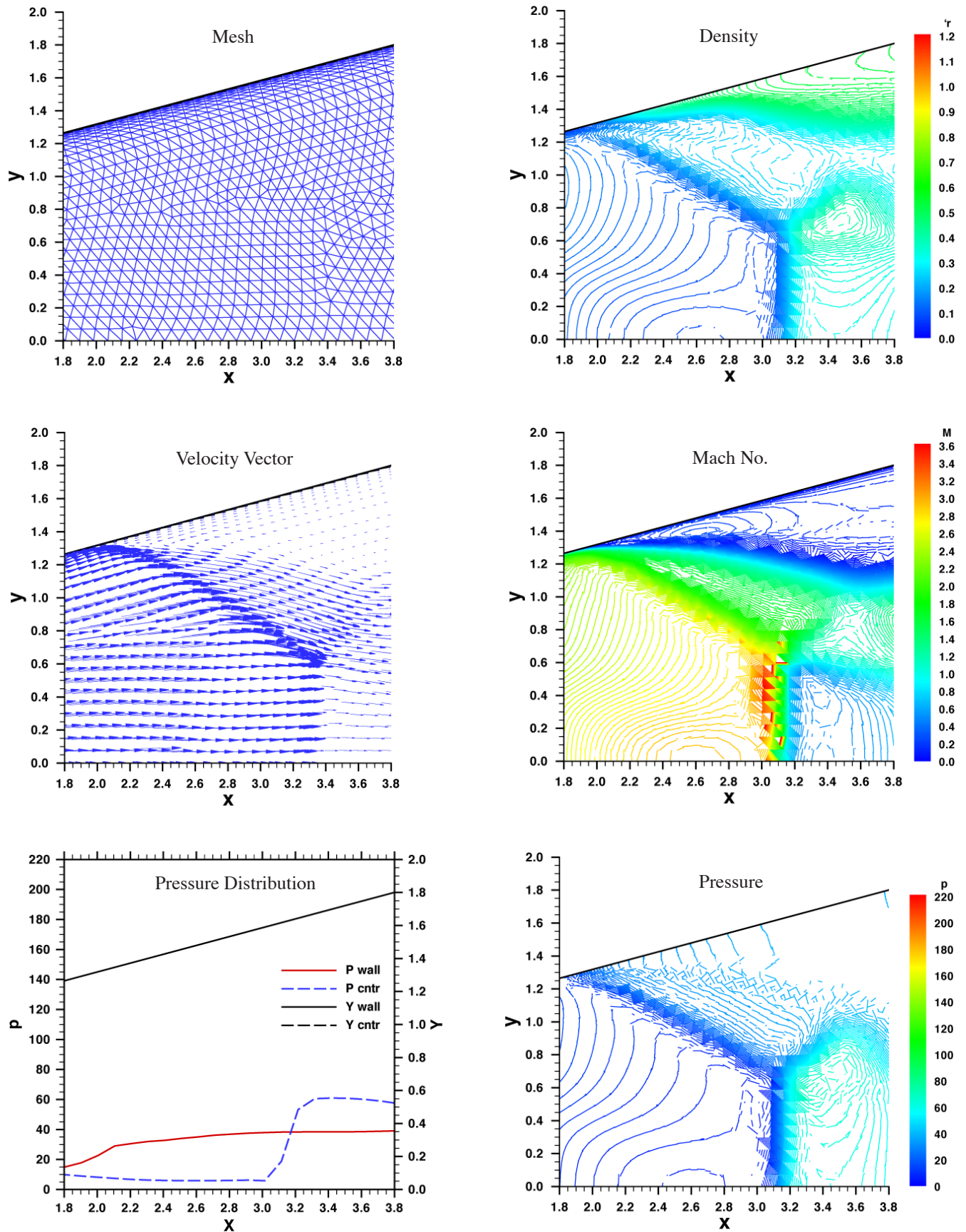


Fig. 6 Mesh and N-S Flow-Field Near Separation Point at Pa/Pt = 0.20

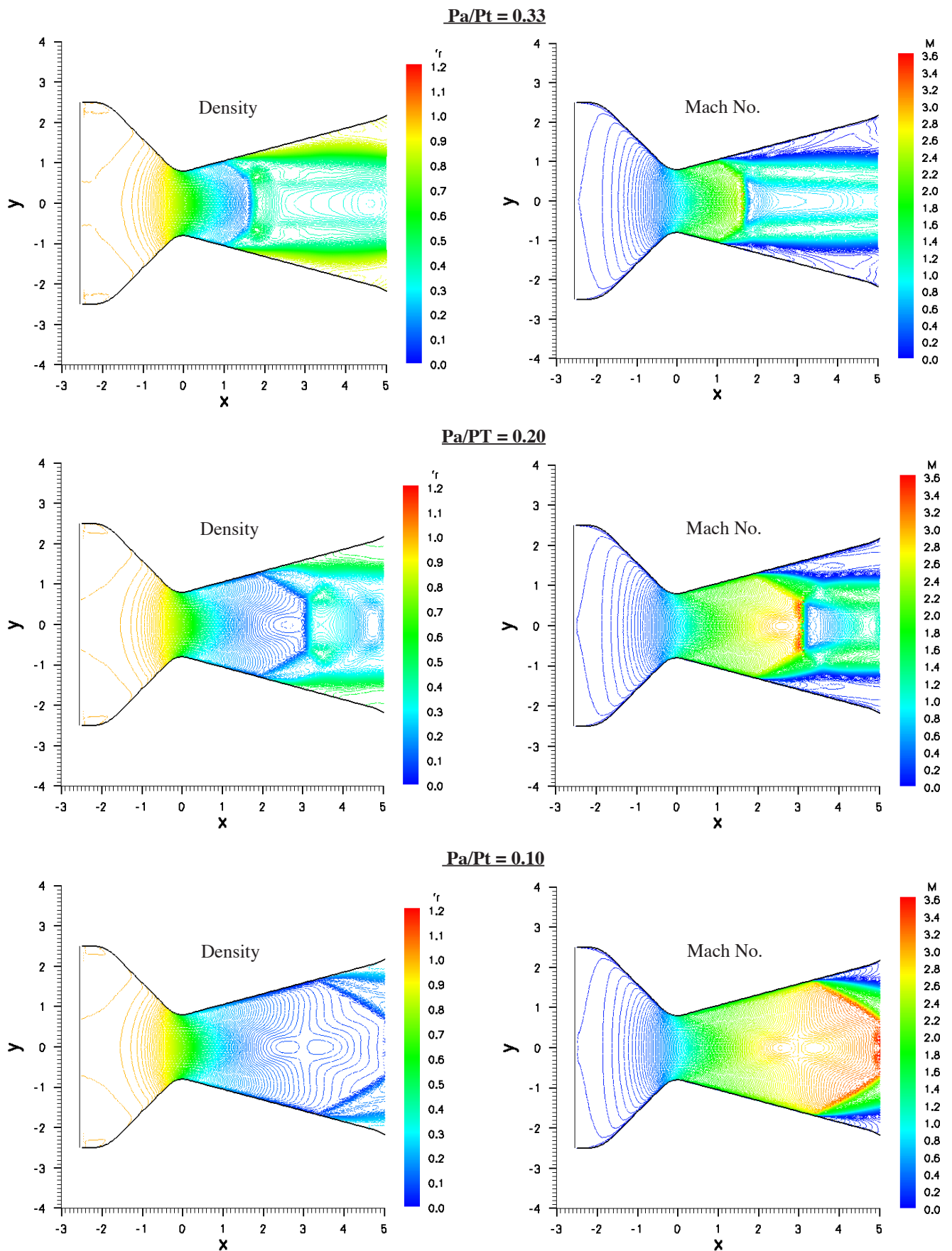


Fig. 7 Established Nozzle Density and Mach No. Contours at $Pa/Pt = 0.33, 0.20, 0.10$

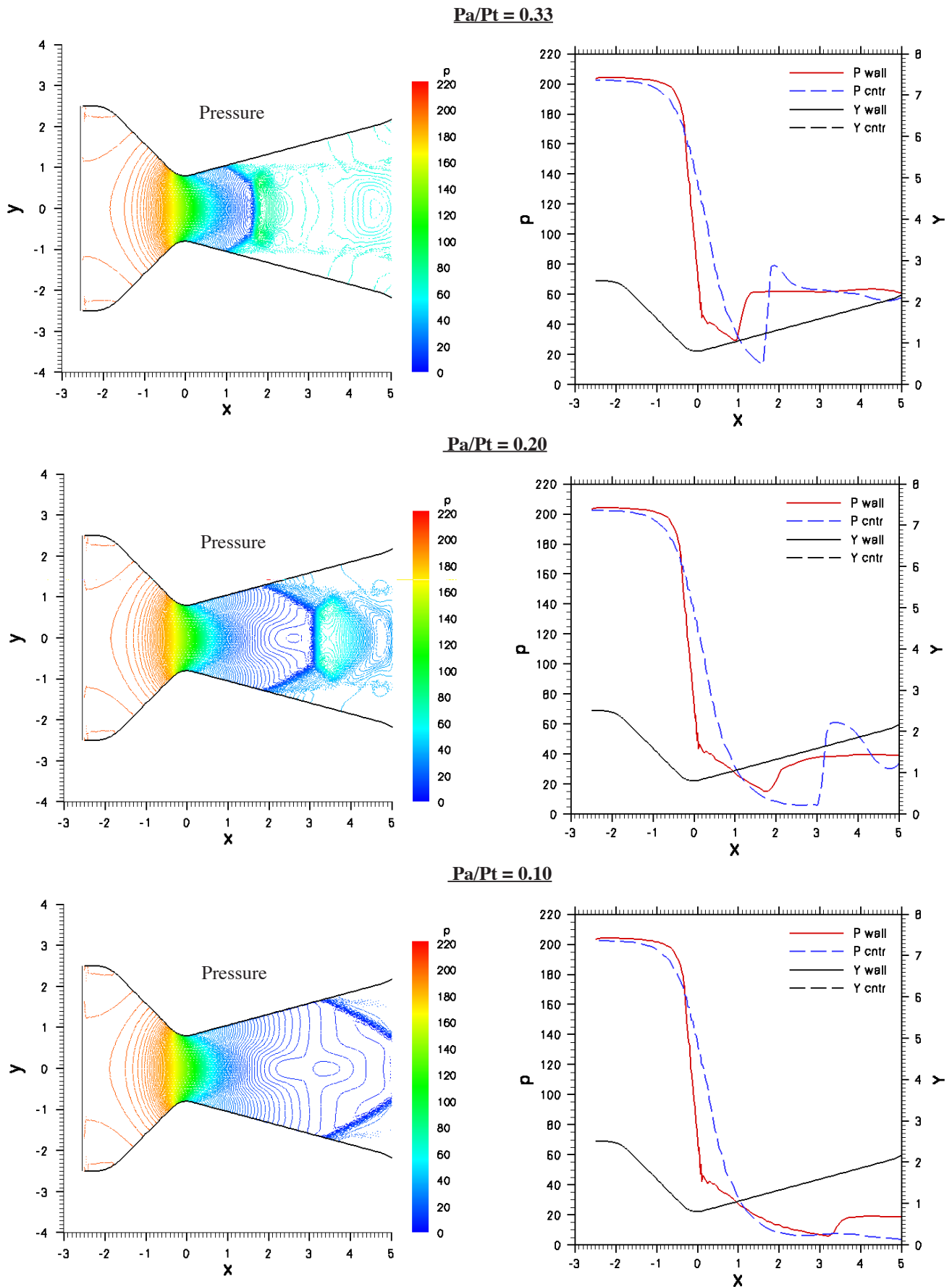


Fig. 8 Established Nozzle Pressure Contours at $P_a/P_t = 0.33, 0.20, 0.10$

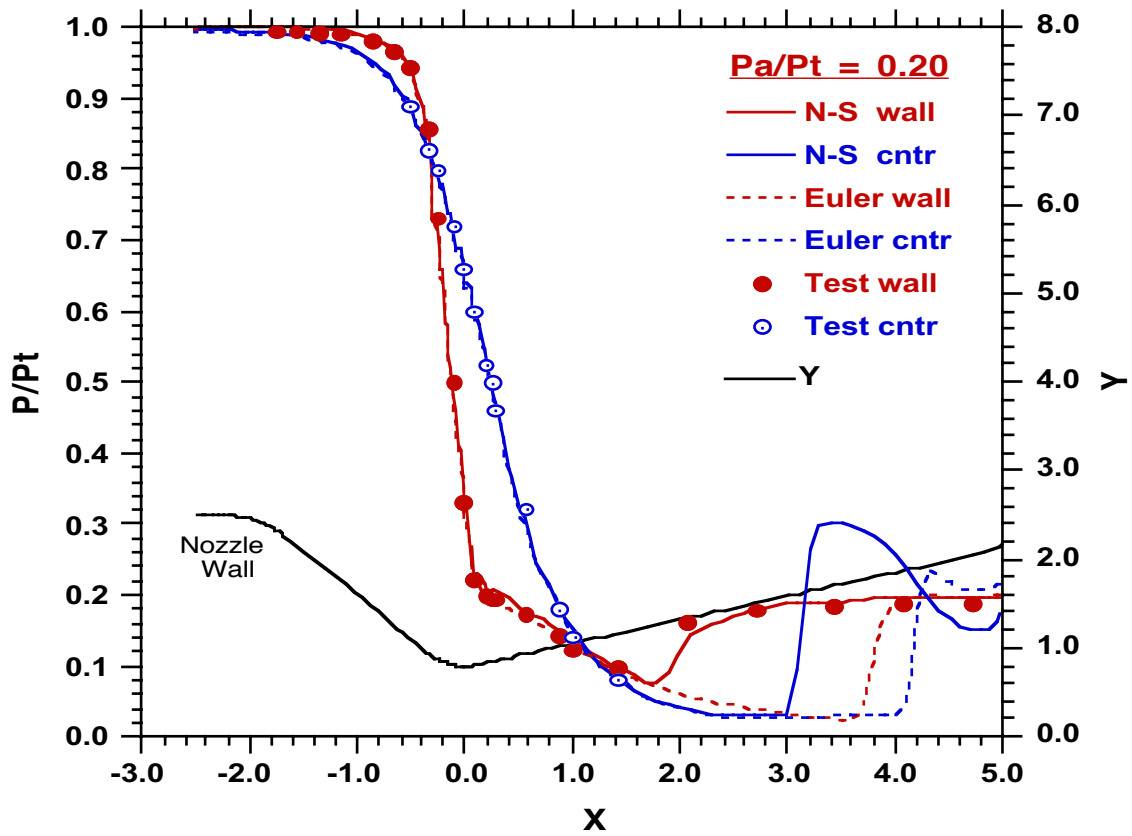


Fig. 9 Pressure Distributions for N-S and Euler Flows at $P_a/P_t = 0.20$

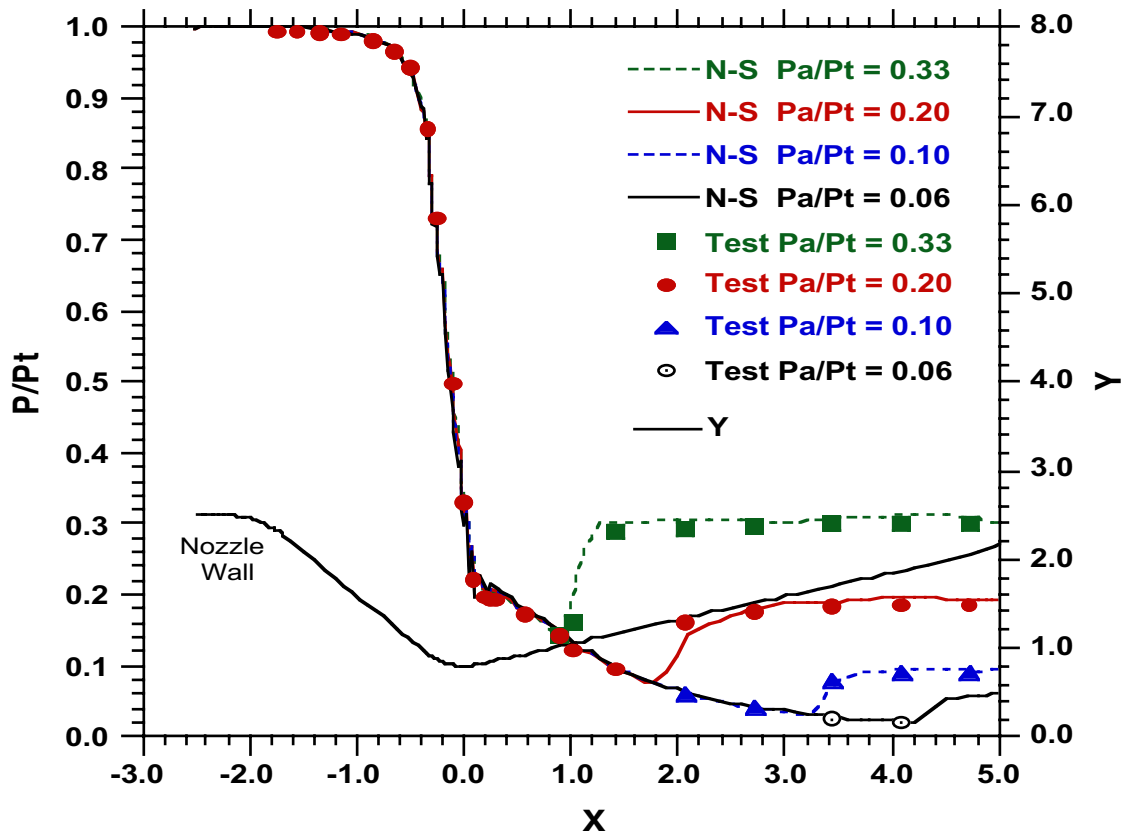


Fig. 10 Flow Separation in Nozzle -- Analysis Results and Test Data